

Learned Inference of Annual Ring Patterns of Solid Wood

paper1019

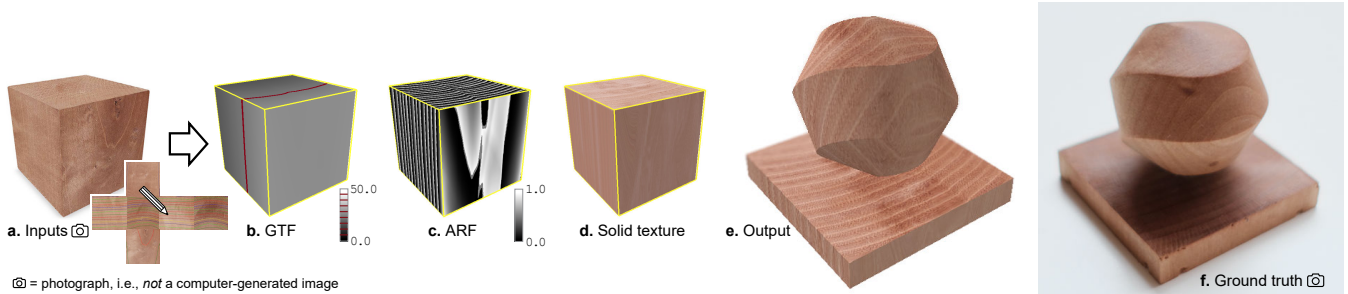


Figure 1: a) Photographs of a wood block and its external surfaces with manually traced annual rings. b) An inferred volumetric growth time field (GTF). c) The GTF is converted to an annual ring field (ARF). d) The ARF is translated to a solid wood texture with realistic colors and detailed features using an orientation-dependent image translation. e) A rendered cut surface. f) The corresponding cut of the physical wood block.

Abstract

We propose a method for inferring the internal anisotropic volumetric texture of a given wood block from annotated photographs of its visible external surfaces. The global structure of the annual ring pattern is represented using a continuous spatial scalar field referred to as the growth time field (GTF). First, we train a generic neural model that can represent various GTFs using procedurally generated training data. Next, we fit the generic model to the GTF of a given wood block based on surface annotations. Additionally, we apply image translation to render orientation-dependent small-scale features and colors on a cut surface. We show rendered results of various real wood samples. A quantitative ablation study on real data demonstrates that our learned model can more robustly infer the internal structure from partial annotations compared to naïve interpolation. Our method can benefit applications such as cut-preview before fabricating solid wood artifacts.

1. Introduction

Solid wood is a ubiquitous material with a characteristic texture that is unique to each material instance. Its modeling includes two aspects: 1) the global structure of the annual ring pattern and 2) the detailed appearance of the local color transitions and detailed features of the material. In this paper, we address these two aspects aiming to infer a solid texture based on the visible exterior surfaces of a physical block of wood (Figure 2). This is useful for predicting the appearance of wood artifacts before fabrication by subtractive manufacturing, such as milling or cutting. The proposed method could enable users to confirm the surface texture pattern, and even choose a material instance or adjust the position and orientation of the artifact inside the material to obtain the most desirable surface texture pattern, based either on strength or on aesthetic criteria (Figure 3). Texture inference could also simplify the material texture design process for artists, especially when it is desirable that the

texture closely resembles a given material exemplar, e.g., in furniture manufacturing.

The inputs to our method are photographs of the six external surfaces of a wood block and annotations on these photographs in the form of traces of the annual rings numbered by year. The output is a volumetric model of the wood block enabling to render a cut surface inside. For the global structure inference, we use a representation that we call growth time field (GTF), a 3D continuous field that represents the time (year) when the growth occurred at each point. The annual rings are implicitly defined by iso-surfaces of the GTF at each whole number. Similar representations have been used for forward modeling of tree growth and annual ring patterns [MPW06,SPH11,KSG^{*}15,LIY^{*}22]. However, we address the inverse problem of inferring the internal volumetric GTF.

For the first aspect—the global structure inference—we first train a generic neural model of GTFs. This model is trained with many procedurally generated GTF samples that cover a wide variety of

annual ring patterns. Then, we infer a specific GTF using the generic model based on annotations tracing annual rings on the six sides of the wood block. Specifically, we search for the latent vector fed to the generic model as well as the position, orientation, and scale of the block within the field that best matches the annual rings by solving an optimization problem.

For the second aspect—local appearance synthesis—the challenge is to replicate realistic colors and detailed features that follow the inferred global structure. Moreover, in the real world, the local appearance of wood material varies depending on in which plane the wood is cut. The end grain—where fibers and pores are facing the surface—tends to be rougher and slightly darker compared to the face grain—where fibers and pores are tangential to the surface (Figure 4). We address these challenges by applying a patch-based image translation method [TFK*20] that transfers the styles of the exterior photographs to the inferred annual ring pattern inside the volume. For the purpose of replicating the anisotropic appearance, we perform the image translations on three orthogonal cross-sections and render a point on a cut surface based on its surface normal. The result of the combined global structure inference and local appearance synthesis is a volumetric solid wood texture corresponding to a physical sample, which can be used to render a cut surface inside the volume with a realistic appearance of the global structure and anisotropic local features.

We evaluate our method on several physical solid wood samples by inferring their volumetric textures, after which we cut the samples to reveal their interior textures. We present these ground truth cut surface textures side-by-side with the corresponding predicted textures for qualitative visual comparison. Based on physical samples with planar cuts, we also present a quantitative ablation and baseline comparison study, which suggests that our method more robustly infers internal structures from partial annotations compared to naive interpolation using the radial basis function (RBF). Furthermore, we show additional visual results comparing orientation-dependent and orientation-agnostic rendering. We also show the effect of changing the orientation of a cut surface inside a wood block and cross-combinations of global structures with different local appearances.

In summary, our contributions are twofold:

- A method for inferring the global volumetric structure of a wood block based on annotated annual rings on the external surface using a learned generic model of annual ring patterns.
- An orientation-dependent rendering method for visualizing the cut surface of a solid wood based on image translation.

2. Related Works

2.1. Tree Growth and Annual Ring Pattern Formation

Tree growth is divided into two types: *apical* and *cambial*. Apical growth elongates the tree and produces new grafting strands, and it is typically modeled with L-systems [GJB*20, Lin68, IOI06]. Cambial growth expands the thickness of the tree by adding a layer of material to its external surface each year, and it is typically simulated using the level set method [KSG*15, MPW06]. This second type of expansion growth gives rise to the annual ring pattern. In

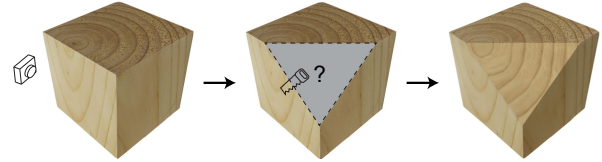


Figure 2: Problem formulation. We aim to infer the internal volumetric texture of solid wood—including the global annual ring structure and local features—given photographs of the exterior surfaces.

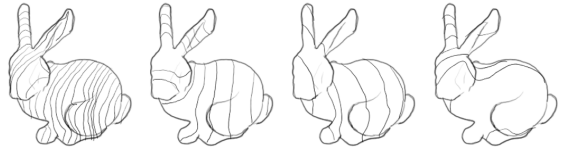


Figure 3: Illustration of variations of appearance of an artifact cut from a solid wood block. The surface pattern varies with the unique material instance and the pose of the artifact inside the material.

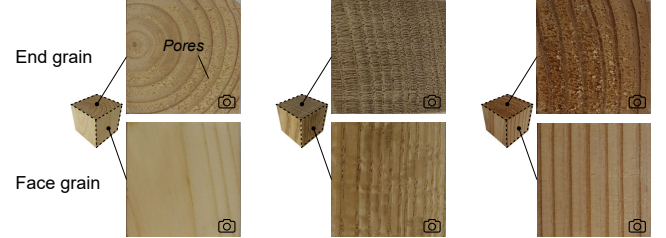


Figure 4: Photographs of different sides of real material samples. Solid Wood exhibits varying local appearances (colors, small-scale features of pores, etc.) on cross-sections in different orientations.

temperate climates, wood grows fast in the spring, adding a thick layer of light material. In the summer and fall, the growth slows down, adding a thin layer of dark material, until stopping completely in the winter. These seasonal shifts in color make the growth layers, i.e., annual rings, visible to the eye. Moreover, various factors (e.g., tree species, sunlight, nutrition) give rise to variations in color and thickness. Therefore, each piece of wood has a unique volumetric texture, even two pieces from the same species are never the same.

2.2. Procedural Wood Texturing

Procedural texturing is a method to generate a texture on demand based on mathematical functions and rules, rather than referring to a stored raster image. Based on this approach, Liu *et al.* [LDHM16] proposed a simulation method to generate a volumetric structure and texture of solid wood. With their method, a user can control various visual features of wood by tuning parameters, such as the distance between annual rings, colors, surface reflectance, and distortions. Moreover, Larsson *et al.* [LIY*22] proposed a method to procedurally model knots and the intricate annual ring distortions they give rise to. These procedural methods are computationally efficient and suitable for many applications, such as in games and videos where

107 the goal is to make the texture look plausible. However, these are
 108 forward methods and do not refer to specific exemplars.

109 The inference of parameters and generation of procedural models
 110 is an active research area [LP00, HGH^{*}22, HHD^{*}22, HDR19,
 111 GHS^{*}22]. For the highly realistic rendering of wood material,
 112 Marschner *et al.* [MWAM05] presented a shading model dealing
 113 with sub-surface highlighting specific to finished wood and a mea-
 114 surement method to obtain rendering parameters from wood samples.
 115 Lefebvre and Poulin [LP00] modeled the structure of wood; specif-
 116 ically, they introduced a procedural wood model with concentric
 117 circular annual rings and extracted its parameters from a 2D image.
 118 Our method is different in that we separate the structure estima-
 119 tion and appearance synthesis, provide a more general annual ring
 120 model, and adopt the image translation for the appearance synthesis.
 121 Moreover, we chose a neural network over a procedural framework
 122 for the inference problem because a neural network is differentiable,
 123 making it easy to fit, while it can be difficult and slow to directly fit
 124 an explicit procedural model to a given input.

125 2.3. Solid Texture Synthesis

126 Another approach to model volumetric materials, including wood
 127 is to synthesize a 3D texture from a 2D reference image using non-
 128 parametric sampling or deep learning. Kopf *et al.* [KFCO^{*}07] syn-
 129 thesized volumetric textures from single 2D images. They extended
 130 a 2D texture optimization method [KEBK05] to 3D and integrated a
 131 histogram matching technique with the texture optimization pro-
 132 cedure. Dong *et al.* [DLTD08] synthesized only parts of the volume
 133 used for rendering and performed pre-computation to reduce the can-
 134 didates of neighborhood matching. They also generated anisotropic
 135 volumes from multiple 2D images. Pietroni *et al.* [POB^{*}07] syn-
 136 thesized a volumetric texture from multiple cross-sectional images
 137 based on a morphing technique. For more related studies, refer to
 138 the survey paper by Pietroni *et al.* [PCOS10].

139 Recently, deep neural network models have been applied to
 140 solid texture synthesis. Gutierrez *et al.* [GRGH18] and Zhao
 141 *et al.* [ZWG^{*}21] adopted generative adversarial networks to synthe-
 142 size solid textures from 2D exemplar images. They introduced multi-
 143 scale representation to their models. Gutierrez *et al.* [GRGH18]
 144 evaluated the similarity between the given exemplars and generated
 145 volumes using their perceptual feature vectors of the images. In
 146 contrast, Zhao *et al.* [ZWG^{*}21] compared 2D patches extracted
 147 from the exemplar and generated volume directly without feature
 148 extraction. Furthermore, Oechsle *et al.* [OMN^{*}19] represented a 3D
 149 texture using a multilayer perceptron (MLP) model that maps 3D
 150 position to appearance. Henzler *et al.* [HMR19] combined the MLP
 151 model with Perlin noise to support an infinite domain and infinite
 152 zoomable synthesis (Figure 5). Portenier *et al.* proposed a similar
 153 noise-based deep neural network (DNN) model [PABG20]. These
 154 methods can synthesize solid textures from 2D exemplars. However,
 155 they focus on local appearances and are therefore most suitable for
 156 globally uniform materials, such as grass and gravel. They do not
 157 reproduce the global structure of wood, i.e., the concentric annual
 158 ring pattern.



Figure 5: Wood texture reconstruction results from deep texture synthesis by Henzler *et al.* [2020]. We use a pre-trained model provided by the authors that is specifically trained on wood, and run it on our wood images.

159 2.4. Neural Surface Modeling

160 Neural implicit surface modeling is a technique to represent 3D
 161 shapes or surfaces implicitly using neural networks. Specifically,
 162 MLP networks define a scalar function $f(\mathbf{z}, \mathbf{x}) \in \mathbb{R}$ that maps a latent
 163 vector \mathbf{z} and 3D position \mathbf{x} to a scalar value. By computing the zero-
 164 level set of this function, a 3D surface model can be obtained. The
 165 versatility of neural implicit modeling allows for the generation of
 166 diverse models by manipulating the latent vector input to the MLP
 167 network. Various methods employ encoder networks to compute
 168 the latent vector [MON^{*}19, CZ19, XWC^{*}19, JSM^{*}20]. Meanwhile,
 169 Park *et al.* [PFS^{*}19] proposed a method to train the distribution
 170 of latent vectors from the dataset using auto-decoder-style training.
 171 Building upon this neural implicit modeling technique proposed
 172 by Park *et al.* [PFS^{*}19], we extend its application to modeling
 173 a volumetric material, moving beyond its conventional usage in
 174 single-view 3D reconstruction and mesh reconstruction from point
 175 clouds.

176 A Neural Radiance Field (NeRF) is another highly effective rep-
 177 resentation that implicitly models the surface geometry and appear-
 178 ance of a shape [MRS^{*}20, MST^{*}20]. Nonetheless, it focuses on
 179 capturing the appearance of the exterior surfaces, rather than the
 180 inside of solid materials.

181 3. Method

182 3.1. Overview

183 Given the exterior surface images of an orthogonal wood block with
 184 annotated annual rings, our goal is to obtain a representation that
 185 recovers its internal structure and render a textured image of a cut
 186 surface. We propose a two-stage method (Figure 6). In the first stage,
 187 we infer the global structure of the annual ring pattern (Section 3.2).
 188 We represent the internal global structure by a GTF. We train a
 189 generic neural model to predict the GTF value at each 3D location
 190 of a wood cuboid. A predicted GTF is then converted into an annual
 191 ring field (ARF) to obtain a volume closer in structure to the actual
 192 layered appearance of wood. In the second stage, we perform local
 193 texture synthesis (Section 3.3). Specifically, we generate an image
 194 translation model for each of three axis orientations and construct
 195 three RGB volumes by applying the image translation models to the
 196 inferred ARF volume. Then, we combine the three RGB volumes to
 197 render a cut surface.

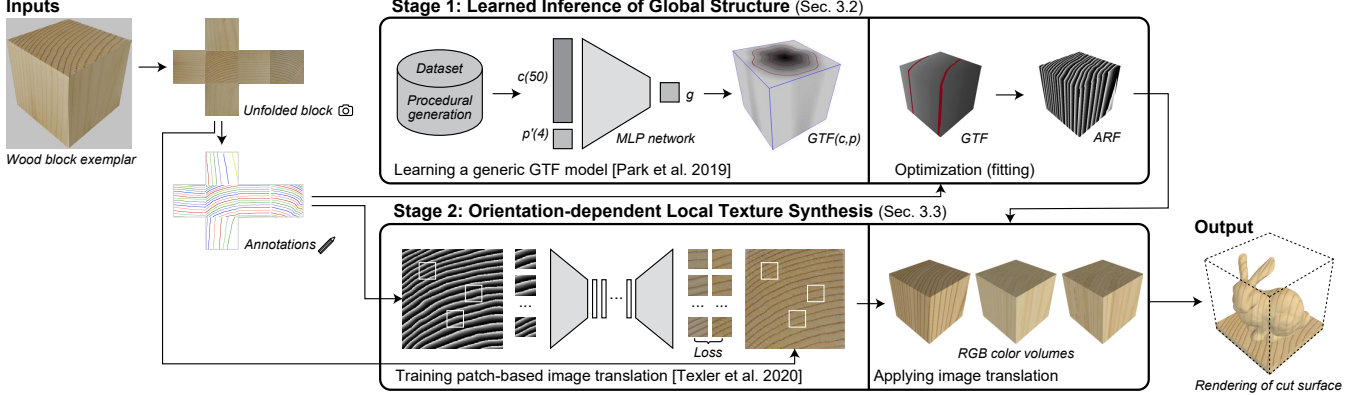


Figure 6: Method overview. The inputs are the external photographs of a wood block annotated with annual ring traces. The method consists of two stages: 1) learned inference of global structure and 2) orientation-dependent local texture synthesis. The output is a rendering of a cut surface inside the wood block.

3.2. Global Structure Inference

3.2.1. Generic Neural GTF Model

In the proposed method, we represent a volumetric annual ring pattern using the GTF

$$GTF(\mathbf{p}) = g : \forall \mathbf{p} \in \mathcal{R}^3, g \in \mathcal{R}, \quad (1)$$

where \mathbf{p} is a 3D point inside a tree with its central axis aligned with the z -axis. The GTF value (g) represents the time when growth occurred relative to the innermost center (pith). We represent a generic model of GTFs using an MLP neural network:

$$f_{\theta}(\mathbf{c}, \mathbf{p}) \approx GTF(\mathbf{p}), \quad (2)$$

where θ represents the network parameters and \mathbf{c} is a latent code. The generic model covers a wide range of GTFs (variations in annual ring patterns) using the latent code to embed the variation in GTFs in a latent space. We inherit the MLP network architecture from Park *et al.* [PFS*19] who developed it for implicit surface modeling via signed distance fields (SDFs), which are similar to GTFs.

3.2.2. Training the Generic Neural GTF Model

During training, we optimize the network parameters θ of our model together with latent codes $\mathbf{c}_i (i = 0, \dots, N)$ for each $GTF_i (i = 0, \dots, N)$ in a procedurally generated training dataset (Section 3.2.4). Given N GTFs, we sample M points from each GTF to obtain pairs $\{(\mathbf{p}_j^i, g_j^i) | i \in (0, 1, \dots, N-1), j \in (0, 1, \dots, M-1)\}$, where $\mathbf{p}_j^i \in \mathcal{R}^3$ is the 3D position of the j th sample point of GTF_i , and g_j^i is its growth time value. Using the sampled training pairs, we optimize $C = \{\mathbf{c}_i\}$ and θ as follows:

$$\arg \min_{C, \theta} \sum_{(i, j)} \|f_{\theta}(\mathbf{c}_i, \gamma(\mathbf{p}_j^i)) - g_j^i\|_1 + w_{\text{reg}} \|\mathbf{c}_i\|_2 \quad (3)$$

where the first term penalizes the deviation of the predicted GTF values from the known GTF values, while the second term regularizes the distribution of latent vectors. To represent the concentric structure of annual ring patterns, we apply a cylindrical positional encoding, which uses a mapping function γ :

$$\gamma(\mathbf{p}) = (r, \arccos(x/r), \arcsin(y/r), z), \quad (4)$$

where $r = \sqrt{x^2 + y^2}$. We set the coefficient $\alpha = 0.01^2$, initialize $\mathbf{z}_i \in \mathcal{R}^{50}$ by sampling from $\mathcal{N}(0, 1/\sqrt{50})$ [PFS*19], and use the Adam optimizer [KB14]. This auto-decoder-style training produces high-quality generative models without requiring an encoder module.

3.2.3. Inferring a GTF

Given six surface images of a wood block with annotated annual ring pixels and their growth time values, our goal is to infer the volumetric GTF that best matches the annotations. We denote the annotated annual ring pixels as (\mathbf{x}_k, g_k) , where $\mathbf{x}_k \in \mathcal{R}^3$ is the location on the external surface of the wood block, and g_k is the growth time value of \mathbf{x}_k . When the pith (innermost tree center) exists on the exterior surface, we set $g_k = 1$ at the innermost annual ring and increment the age from there. When the pith does not exist, we set a tentative value (e.g., $g_k = 10$) for the youngest ring. The age offset is optimized afterwards (refer to Equation 5).

Intuitively, we optimize a latent code vector \mathbf{c} such that the predicted growth time value $f_{\theta}(\mathbf{c}, \mathbf{x}_k)$ matches the annotated growth time (g_k). However, the network models the GTF of a larger portion of a tree truck rather than the block sample (Section 3.2.1). Therefore, it is necessary to optimize a transformation $(\mathcal{T} = (\mathbf{t}, \mathbf{M}, s))$ that represents the cutout location ($\mathbf{t} \in \mathcal{R}^3$), orientation ($\mathbf{M} \in \mathcal{R}^{3 \times 3}$), and relative scale ($s \in R$) of the wood block in the tree trunk portion (Figure 7). The latent vector \mathbf{c} and affine transformation ($\hat{\mathcal{T}}$) are estimated by optimizing

$$\arg \min_{\mathbf{c}, \mathcal{T}, a} \sum_k \|f_{\theta}(\mathbf{c}, \gamma(\mathcal{T}(\mathbf{x}_k))) - (g_k - a)\|_1 + w_{\text{reg}} \|\mathbf{c}\|_2, \quad (5)$$

where $a \in \mathcal{N}$ is an integer value representing an age offset.

We optimize Equation 5 in two steps. First, we fix $\mathbf{c} = \mathbf{0}$ and perform a coarse grid search to obtain \mathbf{t}_0 , \mathbf{m}_0 , s_0 , and a that minimize Equation 5. Next, we initialize the optimization with $\mathbf{c} = \mathbf{0}$, \mathbf{t}_0 , \mathbf{m}_0 , and s_0 and then iteratively optimize Equation 5 while keeping the age offset a fixed. We show an example of visual outputs during the optimization process in Figure 8.

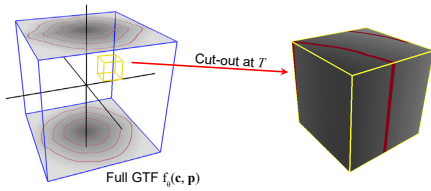


Figure 7: Inferring a GTF. We optimize the latent code c and cutout transformation T .

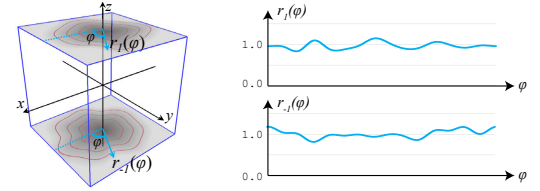


Figure 9: Procedural generation of GTF. We generate a 3D GTF (left) from two radial scaling functions $r_{-1}(\phi)$ and $r_1(\phi)$.

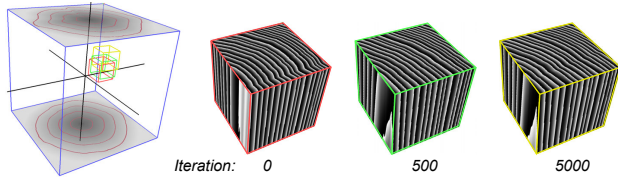


Figure 8: Optimization process. Starting from the coarse grid search result (cube), we iteratively optimize the cutout transformation and latent code.

254 3.3. Local Texture Synthesis

To synthesize the anisotropic local appearance of wood, we propose an orientation-dependent wood texture rendering method using an image translation technique. First, we build three color volumes for the XY-, YZ-, and ZX-cross-sections independently using corresponding image translation models, training a model for each axis orientation (Section 3.3.1). During rendering, we combine the three volumes depending on the normal orientation of a point on the cut surface (Section 3.3.2).

263 3.3.1. Image Translations for Axis-aligned Cross-sections

To perform an image translation considering the annual ring structures, we first convert a GTF to an ARF (annual ring field), which expresses the periodic pattern of the annual rings using the following function:

$$263 \quad ARF(p) = (GTF(p) - \lfloor GTF(p) \rfloor)^2, \quad (9)$$

where $\lfloor \cdot \rfloor$ is the floor function. The ARF has a maximum value at a point where the GTF has a whole value (1.0, 2.0, 3.0, etc.) (Figure 10).

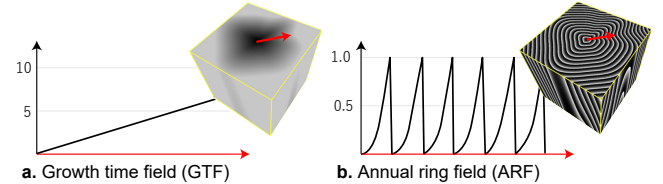


Figure 10: GTF and ARF. The charts plot the values of GTF (a) and ARF (b) along the red arrow.

We build a colored volume for each of the three orthogonal cross-sections by the following process. First, for each side of the cube, a 2D GTF is generated from the annual ring annotations by 2D RBF interpolation. Second, the 2D GTF is converted to 2D ARF, and an image translation network is trained using the image and 2D ARF of the side. (Figure 11-left). Third, the predicted 3D GTF (refer to Section 3.2) is converted into a 3D ARF. Finally, each of the three image translation networks is applied to corresponding cross-sections of the 3D ARF in a given resolution, resulting in three volumetric textures (RGB_{XY} , RGB_{YZ} , and RGB_{ZX}) to be used in Equation 10 below (Figure 11-right). Specifically, we use the patch-based image translation network presented by Texler *et al.* [TFK*20], which can learn a translation mapping between two images. It is based on a network architecture that integrates U-net and ResNet (for details, refer to Texler *et al.* [TFK*20]).

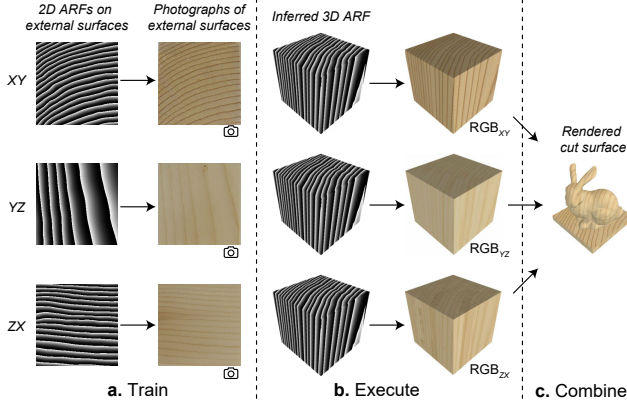


Figure 11: Orientation-dependent image translation. a) For each of three cross-section orientations (XY, YZ, and ZX), we train a network to translate from a 2D ARF on the external surface to a photograph of the same surface. b) Then, we execute the trained models to translate from a predicted ARF volume to RGB volumes. c) Finally, we render a cut surface inside the block by combining the three RGB volumes.

307 a surface model at a real-time rate using [Equation 10](#). Finally, for
308 simplicity, we limited the shape of the input wood block to a cube
309 shape.

310 4.2. Qualitative Evaluation based on Physical Wood Samples

311 For visual evaluation of our outputs, we generated volumetric images
312 of several physical wood samples and visually compared rendered
313 images and photographs ([Figure 1](#), [Figure 12](#)). The samples include
314 various common hard- and softwood species, such as oak and pine.
315 We prepared samples by photographing their external surfaces and
316 manually tracing the annual rings. We then applied our method to
317 generate volumetric color textures and rendered Stanford bunny
318 models. In addition, we physically made various cuts of the wood
319 samples to visually compare the revealed internal textures to those
320 inferred by our method. Planar cuts were made with a saw ([Figure 12](#),
321 wood samples 1-5), while 3D geometries were fabricated using a
322 3D turning machine ([Figure 1](#)) and a 3-axis CNC milling machine
323 ([Figure 12](#), wood samples 6-7), respectively.

324 4.3. Quantitative Evaluation based on Physical Wood Samples

325 Based on the planar cut wood samples from the qualitative evalua-
326 tion ([Figure 12](#), wood samples 1-5), we conducted a quantitative
327 ablation and baseline comparison study to evaluate the accuracy
328 and robustness of our global structure inference method. We pho-
329 tographed the cut surface and manually traced their annual rings
330 while labeling them by year to obtain a ground truth ([Figure 13-left](#)).
331 Then we compared inferred annual ring patterns to the ground truth
332 by measuring what percentage of the points on the inferred annual
333 rings is within a threshold of 2.0 mm from the ground truth.

334 We perform this evaluation on outputs created from full anno-
335 tations, i.e., complete traces of annual rings of all exterior sides,
336 ([Figure 13-middle](#)) and partial annotations, i.e., traces of annual
337 rings on half of the block only ([Figure 13-right](#)). We also compare
338 the outputs of our method to a baseline method of naïve radial basis
339 function (RBF) interpolation. With full annotations, our method
340 has higher average accuracy, and with partial annotations, it con-
341 sistently performs better ([Table 1](#)). The robustness against partial
342 constraints is significant because manually drawing fewer strokes is
343 easier compared to tracing all annual rings on the exterior surface
344 photographs.

Table 1: Quantitative results measuring the percentage of predicted annual ring lines on a cut surface within a threshold of 2.0 mm of the ground truth (refer to [Figure 13](#)).

Wood Sample #	Full annotation		Partial annotation	
	Ours (%)	Baseline (%)	Ours (%)	Baseline (%)
1	86.1	65.9	69.2	58.2
2	99.7	99.5	95.7	66.6
3	28.3	40.6	55.1	22.3
4	92.0	73.6	49.0	30.9
5	99.9	100.0	68.9	58.6
Average	81.2	75.9	67.6	47.3

Moreover, inferring the GTF with our method took one minute

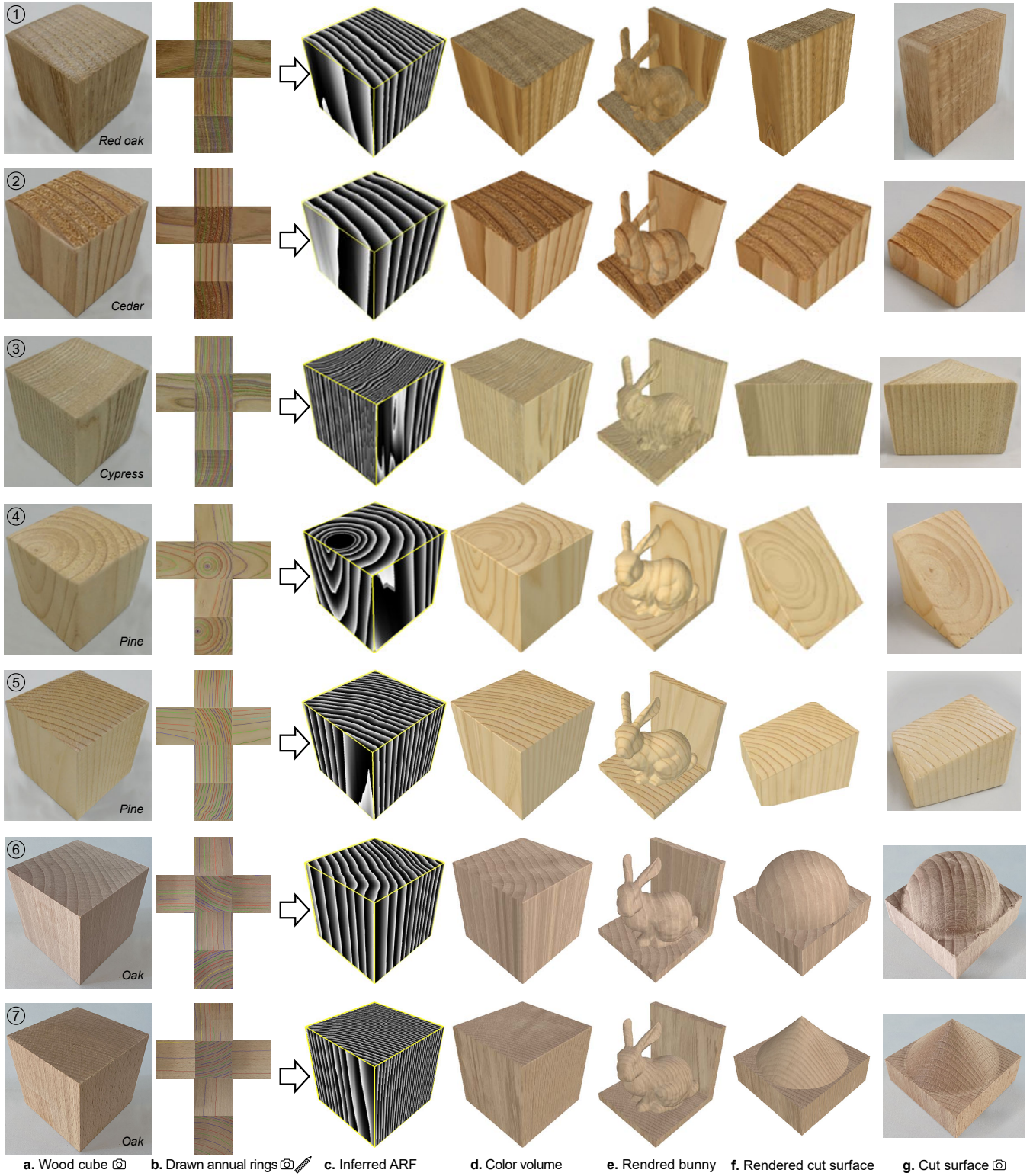


Figure 12: Photographs of five sample wood cubes and volumetric textures generated using our method. Each row shows a photograph of a) a wood cube exemplar, b) its six external surfaces with annotations, c) the inferred ARF, d) color volume after applying image translation, e) a rendered Stanford bunny inside the block, f) and a rendered cut surface corresponding to g) a photograph of a physically cut surface.

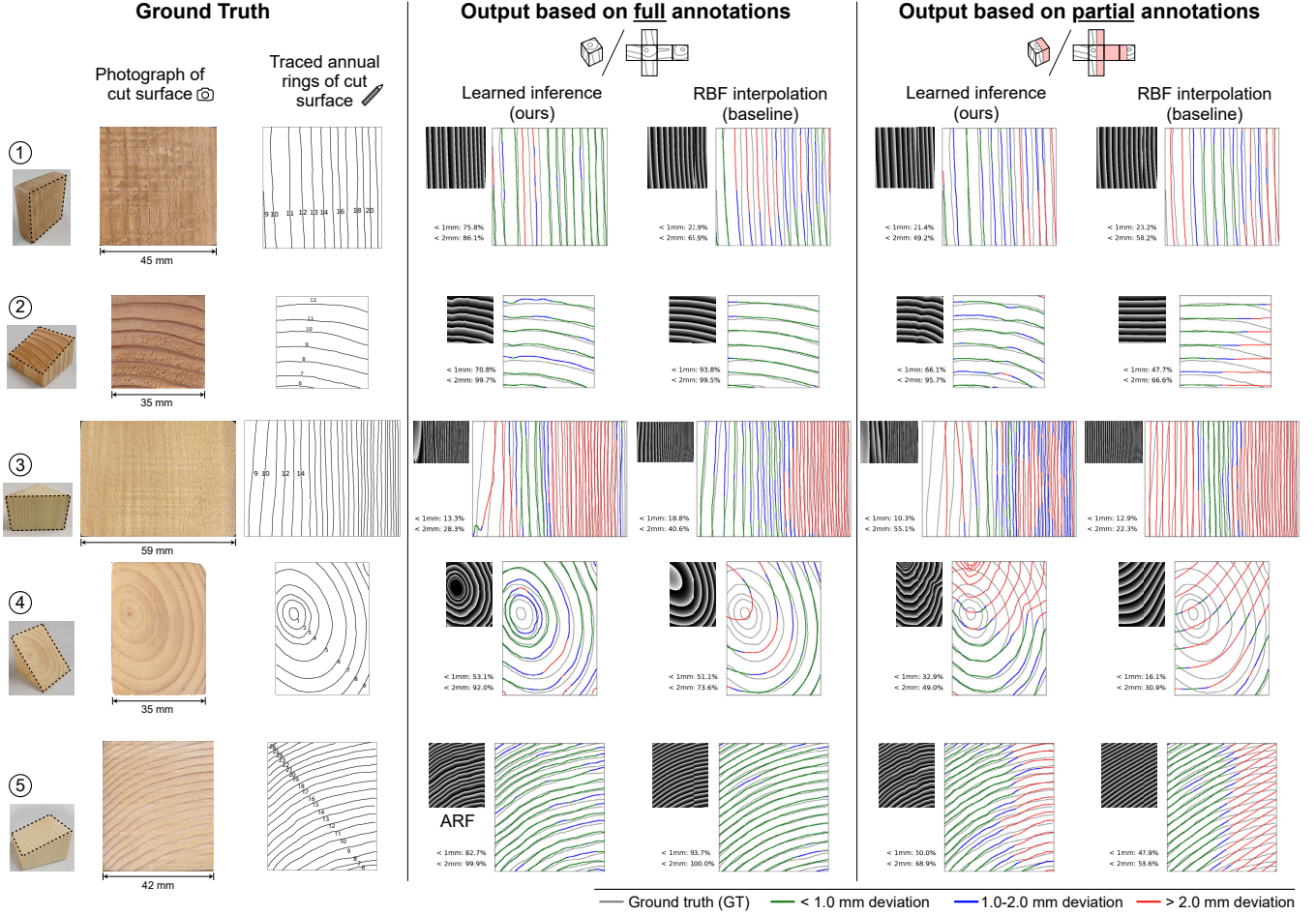


Figure 13: Quantitative ablation and baseline comparison study. Left: the ground truth annual ring pattern of cut surfaces of physical wood samples. Middle: inferred results based on full annotations. Right: inferred results based on partial annotations. For a quantitative compilation, refer to [Table 1](#).

346 on average, while RBF interpolation took three minutes. Note that
 347 these are the computation times of the first step of global inference
 348 only; they do not include the second step (image translation), which
 349 would add to the computation times. Finally, we assume that fur-
 350 ther acceleration is possible because the current implementation is
 351 naively using PyTorch [PGM*19].

352 4.4. Further Experiments

353 A side-by-side comparison between images produced based on our
 354 orientation-dependent and orientation-agnostic renderings shows
 355 that our method better captures the differences between surface
 356 orientations while also producing more natural-looking color varia-
 357 tions ([Figure 16](#)). We also show the effect of varying the orientation
 358 of a cut surface relative to the material ([Figure 15](#)) and what hap-
 359 pens when we apply different local appearances to the same global
 360 structure ([Figure 16](#)).

361 5. Limitations and Future Work

362 Our current method requires an orthogonal cuboid-shaped wood
 363 exemplar. Although the GTF reconstruction could be applied to any
 364 shape, annotating annual rings on arbitrary shapes would be more
 365 challenging. Additionally, our current orientation-dependent ren-
 366 dering method assumes that we can obtain the appearance of three
 367 orthogonal planes of a block shape. In the future, we plan to extend
 368 our method to support arbitrary shapes. Moreover, our method re-
 369 quires manually annotated annual rings for reconstructing the GTF.
 370 It is robust against incomplete annotations (refer to [Section 4.3](#)), but
 371 nevertheless, we plan to develop an automatic annual ring extraction
 372 method based on image translation and edge extraction techniques.

373 Furthermore, our method does not reconstruct small-scale distor-
 374 tions of the GTF appearing on an external surface ([Figure 17a](#)). It
 375 also cannot generate large-scale distortions caused by the grafting
 376 of the tree, such as knots ([Figure 17b](#)). In the future, we plan to
 377 improve the accuracy and diversity of the GTF reconstruction by
 378 increasing the training dataset diversity. Moreover, as for evalua-
 379 tion of the inferred pattern, our quantitative study is based on five

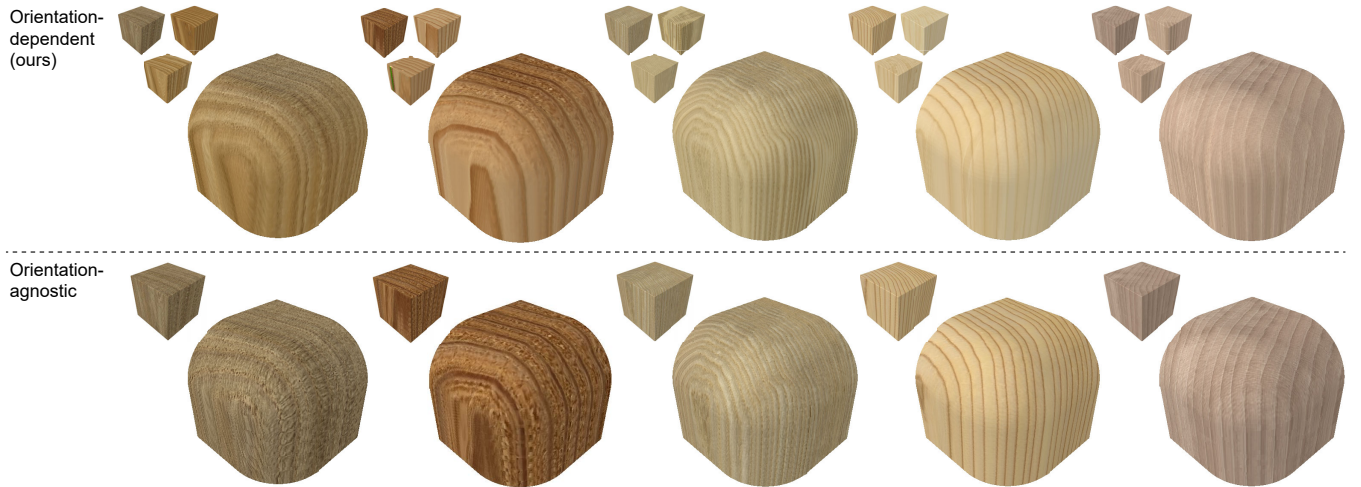


Figure 14: Top: Orientation-dependent rendering mixes three color volumes constructed from the XY, YZ, and ZX cross sections, respectively, based on the normal direction of a point on the cut surface. Bottom: Orientation-agnostic rendering samples one color volume constructed from the XY cross-section. The orientation-dependent rendering better preserves local anisotropic appearances and gives a more natural color variation.

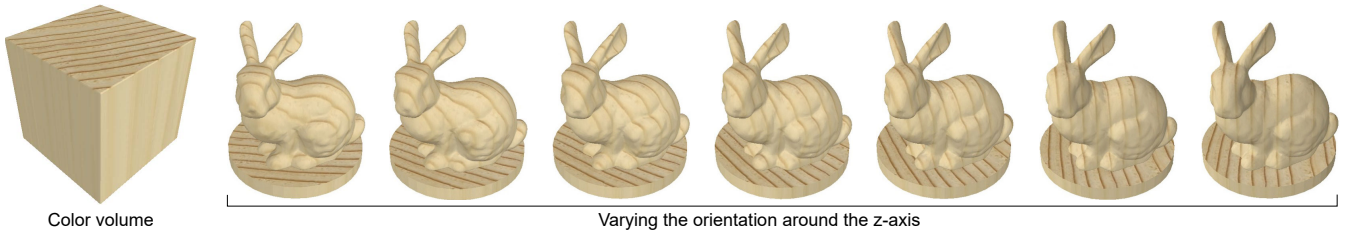


Figure 15: The cut surface is rotated incrementally around the z-axis relative to the material by 15 degrees. This changes the annual ring pattern on the surface.

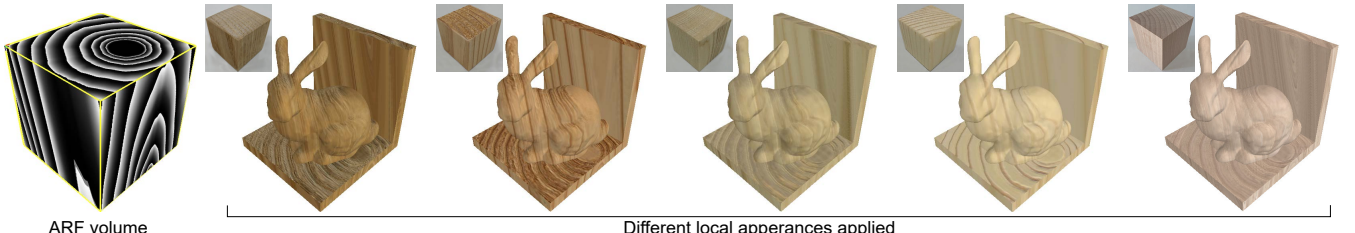


Figure 16: Cut surfaces with the same ARF (global structure) but different local appearances. These cross-combinations are possible because of the separation of the two steps of the method—global structure inference and local texture synthesis.

samples from four different wood species. In the future, it would be desirable to create a dataset of a larger quantity of samples from a wider variety of wood species to enable more extensive evaluation.

Moreover, although rare, the image translation produces unsatisfactory results when the annual rings on an external surface are too sparse (Figure 18). This is because the image translation is trained using small patches of the input images, and some of the patches do not contain any annual rings if they are too sparse. Moreover, it is computationally costly to train multiple image translation models for each sample. In the future, we plan to investigate how to learn a

single conditional image translation model for each type of wood and use it for the reconstruction of the local appearance. On one hand, this could accelerate the image translation process and mitigate failure cases caused by too few rings (Figure 18). On the other hand, it might yield poorer results when applied to wood samples that significantly deviate from the appearance of those in the training dataset.

It is common to decompose complex models into multiple parts due to constraints in CNC fabrication of wood artifacts [MLS*18, HMA15]. Inferring the internal pattern using our method can help

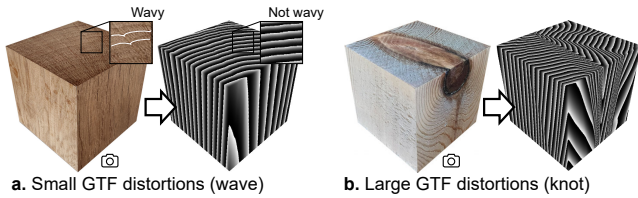


Figure 17: Failure cases. Our method does not succeed in reproducing a) very small or b) very large distortions of the GTF.



Figure 18: Failure case. The image translation gives unsatisfactory outputs when the annual rings are too sparse on an external surface. The white box indicates a patch without structural information.

systems in matching the texture of the parts for improved appearance of the assembled artifact. This is similar to previous systems matching patterns over garment seams [WSH19]. Another possible future application is to complement shape completion with material texture completion for cases when there is an incomplete 3D scan of a solid wood object. Moreover, previous work proposed a method for strength-optimization of the orientation of artifacts fabricated using Fused Deposition Modeling (FDM) 3D printing, leveraging the anisotropic property of the filament bounds [US13]. A similar technique could be applied to increase the strength of wood artifacts fabricated by CNC milling or similar methods, after obtaining a model of its volumetric structure.

6. Conclusion

In this paper, we proposed the first learned model for inferring the volumetric global structure of the annual rings of solid wood. Compared to a baseline of basic interpolation, we showed that our global inference method is marginally more accurate under full annotations and substantially better under partial annotations, while being three times faster. We further proposed a novel orientation-dependent rendering method that replicates the anisotropic appearance of the local features and colors. In conclusion, the proposed workflow involves constructing a model of a natural phenomenon through learning and employing it for reconstruction. This approach is widely applicable and holds significant potential for inspiring further research in a variety of domains.

References

- [CZ19] CHEN Z., ZHANG H.: Learning implicit fields for generative shape modeling. In *Proceedings of the IEEE/CVF Conference on Computer Vision and Pattern Recognition (CVPR)* (June 2019). 3
- [DLTD08] DONG Y., LEFEBVRE S., TONG X., DRETTAKIS G.: Lazy solid texture synthesis. In *Proceedings of the Nineteenth Eurographics conference on Rendering* (Aire-la-Ville, Switzerland, Switzerland, 2008), EGSR’08, Eurographics Association, pp. 1165–1174. doi:10.1111/j.1467-8659.2008.01254.x. 3
- [GBGB95] GRÖNLUND A., BJÖRKLUND L., GRUNDBERG S., BERGGREN G.: *Manual för furustambank*. Tech. rep., Luleå Technical University, 1995. 5
- [GHS*22] GUERRERO P., HAŠAN M., SUNKAVALLI K., MĚCH R., BOUBEKEUR T., MITRA N. J.: Matformer: A generative model for procedural materials. *ACM Trans. Graph.* 41, 4 (jul 2022). URL: <https://doi.org/10.1145/3528223.3530173>, doi:10.1145/3528223.3530173. 3
- [GJB*20] GUO J., JIANG H., BENES B., DEUSSEN O., ZHANG X., LISCHINSKI D., HUANG H.: Inverse procedural modeling of branching structures by inferring l-systems. *ACM Trans. Graph.* 39, 5 (jun 2020). URL: <https://doi.org/10.1145/3394105>, doi:10.1145/3394105. 2
- [GRGH18] GUTIERREZ J., RABIN J., GALERNE B., HURTUT T.: On Demand Solid Texture Synthesis Using Deep 3D Networks. working paper or preprint, Dec. 2018. URL: <https://hal.archives-ouvertes.fr/hal-01678122>. 3
- [HDR19] HU Y., DORSEY J., RUSHMEIER H.: A novel framework for inverse procedural texture modeling. *ACM Trans. Graph.* 38, 6 (nov 2019). URL: <https://doi.org/10.1145/3355089>, doi:10.1145/3355089.3356516. 3
- [HGH*22] HU Y., GUERRERO P., HASAN M., RUSHMEIER H., DESCHAINTRE V.: Node graph optimization using differentiable proxies. In *ACM SIGGRAPH 2022 Conference Proceedings* (New York, NY, USA, 2022), SIGGRAPH ’22, Association for Computing Machinery. URL: <https://doi.org/10.1145/3528233.3530733>, doi:10.1145/3528233.3530733. 3
- [HHD*22] HU Y., HE C., DESCHAINTRE V., DORSEY J., RUSHMEIER H.: An inverse procedural modeling pipeline for svbrdf maps. *ACM Trans. Graph.* 41, 2 (jan 2022). URL: <https://doi.org/10.1145/3502431>, doi:10.1145/3502431. 3
- [HMA15] HERHOLZ P., MATUSIK W., ALEXA M.: Approximating free-form geometry with height fields for manufacturing. *Comput. Graph. Forum* 34, 2 (may 2015), 239–251. URL: <https://doi.org/10.1111/cgf.12556>, doi:10.1111/cgf.12556. 9
- [HMR19] HENZLER P., MITRA N. J., RITSCHEL T.: Learning a neural 3d texture space from 2d exemplars. In *The IEEE Conference on Computer Vision and Pattern Recognition (CVPR)* (June 2019). 3
- [IOI06] IJIRI T., OWADA S., IGARASHI T.: The sketch L-system: Global control of tree modeling using free-form strokes. In *Lecture Notes in Computer Science (including subseries Lecture Notes in Artificial Intelligence and Lecture Notes in Bioinformatics)* (2006), vol. 4073 LNCS. doi:10.1007/11795018(_)_13. 2
- [JSM*20] JIANG C., SUD A., MAKADIA A., HUANG J., NIESSNER M., FUNKHOUSER T.: Local implicit grid representations for 3d scenes. In *IEEE Conference on Computer Vision and Pattern Recognition (CVPR)* (2020). 3
- [KB14] KINGMA D. P., BA J.: Adam: A method for stochastic optimization. *arXiv preprint arXiv:1412.6980* (2014). 4
- [KEBK05] KWATRA V., ESSA I., BOBICK A., KWATRA N.: Texture optimization for example-based synthesis. In *ACM SIGGRAPH 2005 Papers* (New York, NY, USA, 2005), SIGGRAPH ’05, Association for Computing Machinery, p. 795–802. URL: <https://doi.org/10.1145/1186822.1073263>, doi:10.1145/1186822.1073263. 3
- [KFCO*07] KOPF J., FU C.-W., COHEN-OR D., DEUSSEN O., LISCHINSKI D., WONG T.-T.: Solid texture synthesis from 2d exemplars. *ACM Trans. Graph.* 26, 3 (jul 2007), 2–es. URL: <https://doi.org/10.1145/1276377.1276380>, doi:10.1145/1276377.1276380. 3
- [KSG*15] KRATT J., SPICKER M., GUAYAQUIL A., FISER M., PIRK S., DEUSSEN O., HART J. C., BENES B.: Woodification: User-Controlled Cambial Growth Modeling. *Computer Graphics Forum* (2015). doi:10.1111/cgf.12566. 1, 2

- 498 [LDHM16] LIU A. J., DONG Z., HAŠAN M., MARSCHNER S.: Simulating the structure and texture of solid wood. *ACM Trans. Graph.* 35, 6 (nov 500 2016). URL: <https://doi.org/10.1145/2980179.2980255>. 2
- 501
- 502 [Lin68] LINDENMAYER A.: Mathematical models for cellular interactions 503 in development I. Filaments with one-sided inputs. *Journal of Theoretical 504 Biology* 18, 3 (1968). doi:10.1016/0022-5193(68)90079-9. 2
- 505 [LIY*22] LARSSON M., IJIRI T., YOSHIDA H., HUBER J. A. J., 506 FREDRIKSSON M., BROMAN O., IGARASHI T.: Procedural texturing 507 of solid wood with knots. *ACM Trans. Graph.* 41, 4 (jul 2022). 508 URL: <https://doi.org/10.1145/3528223.3530081>, doi: 509 10.1145/3528223.3530081. 1, 2
- 510 [LP00] LEFEBVRE L., POULIN P.: Analysis and synthesis of structural 511 textures. In *Graphics Interface 2000* (May 2000), pp. 77–86. 3
- 512 [MLS*18] MUNTONI A., LIVESU M., SCATENI R., SHEFFER A., 513 PANIZZO D.: Axis-aligned height-field block decomposition of 3d 514 shapes. *ACM Trans. Graph.* 37, 5 (oct 2018). URL: <https://doi.org/10.1145/3204458>. 9
- 515
- 516 [MON*19] MESCHEDER L., OECHSLE M., NIEMEYER M., NOWOZIN 517 S., GEIGER A.: Occupancy networks: Learning 3d reconstruction in 518 function space. In *Proceedings of the IEEE/CVF Conference on Computer 519 Vision and Pattern Recognition (CVPR)* (June 2019). 3
- 520 [MPW06] MANN J., PLANK M., WILKINS A.: Tree growth and wood 521 formation — applications of anisotropic surface growth. In *Proceedings 522 of the Mathematics in Industry Study Group* (2006), pp. 153–192. 1, 2
- 523 [MRS*20] MARTIN-BRUALLA R., RADWAN N., SAJJADI M. S. M., 524 BARRON J. T., DOSOVITSKIY A., DUCKWORTH D.: Nerf in the 525 wild: Neural radiance fields for unconstrained photo collections. *CoRR 526 abs/2008.02268* (2020). URL: <https://arxiv.org/abs/2008.02268>, arXiv:2008.02268. 3
- 527
- 528 [MST*20] MILDENHALL B., SRINIVASAN P. P., TANCIK M., BARRON 529 J. T., RAMAMOORTHI R., NG R.: Nerf: Representing scenes as neural 530 radiance fields for view synthesis. In *Computer Vision – ECCV 2020: 16th 531 European Conference, Glasgow, UK, August 23–28, 2020, Proceedings, 532 Part I* (Berlin, Heidelberg, 2020), Springer-Verlag, p. 405–421. URL: 533 https://doi.org/10.1007/978-3-030-58452-8_24, doi: 534 10.1007/978-3-030-58452-8_24. 3
- 535 [MWAM05] MARSCHNER S. R., WESTIN S. H., ARBREE A., MOON 536 J. T.: Measuring and modeling the appearance of finished wood. 537 In *ACM SIGGRAPH 2005 Papers* (New York, NY, USA, 2005), 538 SIGGRAPH ’05, Association for Computing Machinery, p. 727–734. 539 URL: <https://doi.org/10.1145/1186822.1073254>, doi: 540 10.1145/1186822.1073254. 3
- 541 [OMN*19] OECHSLE M., MESCHEDER L. M., NIEMEYER M., 542 STRAUSS T., GEIGER A.: Texture fields: Learning texture representations 543 in function space. *2019 IEEE/CVF International Conference on Computer 544 Vision (ICCV)* (2019), 4530–4539. 3
- 545 [PABG20] PORTENIER T., ARJOMAND BIGDELI S., GOKSEL 546 O.: Gramgan: Deep 3d texture synthesis from 2d exemplars. 547 In *Advances in Neural Information Processing Systems* (2020), 548 Larochelle H., Ranzato M., Hadsell R., Balcan M., Lin H., (Eds.), 549 vol. 33, Curran Associates, Inc., pp. 6994–7004. URL: <https:////proceedings.neurips.cc/paper/2020/file/4df5bde009073d3ef60da64d736724d6-Paper.pdf>. 3
- 550
- 553 [PCOS10] PIETRONI N., CIGNONI P., OTADUY M., SCOPIGNO R.: 554 Solid-texture synthesis: A survey. *IEEE Computer Graphics and Applications* 555 30, 4 (2010), 74–89. doi:10.1109/MCG.2009.153. 3
- 556 [PFS*19] PARK J. J., FLORENCE P., STRAUB J., NEWCOMBE R., LOVE- 557 GROVE S.: Deepsdf: Learning continuous signed distance functions 558 for shape representation. In *Proceedings of the IEEE Computer Society Conference on Computer Vision and Pattern Recognition* (2019), 559 vol. 2019-June. doi:10.1109/CVPR.2019.00025. 3, 4
- 560
- 561 [PGM*19] PASZKE A., GROSS S., MASSA F., LERER A., BRADBURY 562 J., CHANAN G., KILLEEN T., LIN Z., GIMELSHEIN N., ANTIGA L., 563 DESMAISON A., KOPF A., YANG E., DEVITO Z., RAISON M., TEJANI 564 A., CHILAMKURTHY S., STEINER B., FANG L., BAI J., CHINTALA 565 S.: Pytorch: An imperative style, high-performance deep learning library. In *Advances in Neural Information Processing Systems 32*. Curran Associates, Inc., 2019, pp. 8024–8035. 6, 8
- 566
- 567
- 568 [POB*07] PIETRONI N., OTADUY M. A., BICKEL B., GANOVELLI F., 569 GROSS M.: Texturing Internal Surfaces from a Few Cross Sections. 570 *Computer Graphics Forum* (2007). doi:10.1111/j.1467-8659. 571 2007.01087.x. 3
- 572
- 573 [SPH11] SELLIER D., PLANK M. J., HARRINGTON J. J.: A mathematical 574 framework for modelling cambial surface evolution using a level set method. *Annals of Botany* 108, 6 (2011). doi:10.1093/aob/mcr067. 1
- 575
- 576 [TFK*20] TEXLER O., FUTSCHIK D., KUČERA M., JAMRIŠKA O., SO- 577 CHOROVÁ V., CHAI M., TULYAKOV S., SYKORA D.: Interactive style 578 transfer to live video streams. *SIGGRAPH ’20*, Association for Com- 579 puting Machinery. URL: <https://doi.org/10.1145/3407662.3407752>, doi:10.1145/3407662.3407752. 2, 5
- 580
- 581 [US13] UMETANI N., SCHMIDT R.: Cross-sectional structural analysis 582 for 3d printing optimization. In *SIGGRAPH Asia 2013 Technical Briefs* 583 (New York, NY, USA, 2013), SA ’13, Association for Computing Machinery. URL: <https://doi.org/10.1145/2542355.2542361>, 584 doi:10.1145/2542355.2542361. 10
- 585
- 586 [WSH19] WOLFF K., SORKINE-HORNUNG O.: Wallpaper pattern align- 587 ment along garment seams. *ACM Trans. Graph.* 38, 4 (jul 2019). 588 URL: <https://doi.org/10.1145/3306346.3322991>, doi: 589 10.1145/3306346.3322991. 10
- 590
- 591 [XWC*19] XU Q., WANG W., CEYLAN D., MECH R., NEUMANN 592 U.: Disn: Deep implicit surface network for high-quality single-view 593 3d reconstruction. In *Advances in Neural Information Processing Systems* 594 (2019), Wallach H., Larochelle H., Beygelzimer A., d’Alché-Buc 595 F., Fox E., Garnett R., (Eds.), vol. 32, Curran Associates, Inc. URL: 596 <https://proceedings.neurips.cc/paper/2019/file/39059724f73a9969845dfe4146c5660e-Paper.pdf>. 3
- 597
- 598 [ZWG*21] ZHAO X., WANG L., GUO J., YANG B., ZHENG J., LI F.: 599 Solid texture synthesis using generative adversarial networks. *CoRR 600 abs/2102.03973* (2021). URL: <https://arxiv.org/abs/2102.03973>, arXiv:2102.03973. 3